Materials Science in Semiconductor Processing 30 (2015) 592–598

Contents lists available at ScienceDirect

Materials Science in Semiconductor Processing

journal homepage: www.elsevier.com/locate/mssp

Enhanced photocatalytic activity of graphene oxide/titania nanosheets composites for methylene blue degradation

Xinning Luan [a], M. Teresa Gutierrez Wing [b], Ying Wang [a,*]

[a] Department of Mechanical and Industrial Engineering, Louisiana State University, Baton Rouge, LA 70803, USA
[b] Department of Civil and Environmental Engineering, Louisiana State University, Baton Rouge, LA 70803, USA

ARTICLE INFO

Available online 24 November 2014

Keywords:
TiO_2 nanosheet
Chemical exfoliation
Graphene oxide
Photocatalytic activity

ABSTRACT

In the present work, we report enhanced photocatalytic degradation of methylene blue dye in aqueous solution by using ultra-thin anatase TiO_2 nanosheets (NSs) combined with graphene oxide (GO) as a photocatalyst. The two-dimensional ultra-thin anatase TiO_2 NSs are fabricated via chemical exfoliation. By completely delaminating a lepidocrocite-type layered protonic titanate $H_xTi_{2-x/4}\square_{x/4}O_4 \cdot H_2O$ ($x=0.7$, □: vacancy) into individual layers through ion exchange with tetrabutylammonium (TBA^+) cations, well-dispersed ultra-thin colloidal $Ti_{0.91}O_2$ NSs with a lateral size up to a few micrometers are obtained. Subsequent acid treatment induces colloidal $Ti_{0.91}O_2$ to reassemble and precipitate into a gelation form, followed by thermal annealing to convert the $Ti_{0.91}O_2$ gelation into anatase TiO_2 nanosheets as photocatalyst for methylene blue degradation. TiO_2 NSs show a high photocatalytic degradation efficiency of 53.2% due to the ultra-thin thickness for facile electron transfering and large surface area for methylene blue absorption. Moreover, photocatalytic effect can be further improved by simply adding GO suspension to achieve colloidal self-assembly of GO and TiO_2 NSs. An optimal GO content of 3 wt% further increases the photocatalytic degradation efficiency to 91.2% due to faster electron–hole seperation and improved surface area provided by GO. This work provides a simple but effective approach by combing graphene oxide with TiO_2 nanosheets synthesized via the exfoliation method for methylene blue degradation.

1. Introduction

Research on semiconductor photocatalysis has attracted much interest due to an increasing demand of environmental remediation. Semiconducting titanium dioxide (TiO_2) has attracted considerable attention in the field of photocatalysis due to its chemical stability, non-toxicity, and readily available raw materials. It also finds wide applications in the fields of renewable energy, electrochemical energy and environmental protection such as dye-sensitized solar cells (DSSCs) [1–5], gas sensing [6–8], water splitting [9,10], biomedical materials [11,12], and lithium-ion batteries [13]. However, there are two major factors limiting application of TiO_2 in photocatalysis: (i) recombination of most of photogenerated electron–hole due to low mobility of charge carriers when migrating to the catalyst surface (e–h) pairs, and (ii) relatively large band gap which determines the energy necessary to create e–h pairs in the semiconductor for promoting photocatalytic processes.

Nanostructured TiO_2 photocatalyst with tailored features shows a higher photocatalyisis efficiency due to its effect on reducing e–h recombination rate [14–16]. Two-dimensional (2D) TiO_2 nanosheet (NS) is particularly interesting owing to several advantages described as follows. First, TiO_2 NS can

* Corresponding author. Tel.: +1 225 578 8577; fax: +1 225 578 5924.
E-mail address: ywang@lsu.edu (Y. Wang).

http://dx.doi.org/10.1016/j.mssp.2014.10.032
1369-8001/

serve as a hosting material to load guest functional nanomaterials and the resulting nanocomposite structure has advantages of both components in addition to other unique new properties. Second, 2D TiO_2 NSs and its derived nanocomposite materials can transform from 2D to 1D structure by scrolling into nanorolls or nanotubes [17]. Third, TiO_2 NS, especially ultra-thin TiO_2 NS, provides large interaction area between TiO_2 catalysts and organic pollutants. Since photocatalytic reactions mainly occur on the surface of photocatalyst, thus TiO_2 NS with large surface area will show higher degradation efficiency. Therefore, TiO_2 NSs demonstrate as a very promising catalyst for photocatalytic reactions. TiO_2 NSs can usually be synthesized via hydrothermal method using titanium salts as the precursor and hydrofluoric acid as the solvent [18,19]. However, hydrofluoric acid used in this hydrothermal method is corrosive and needs to be handled with extreme care. Another disadvantage is that the hydrothermal method relying on sealed autoclaves limits its application in large scale production of TiO_2 NSs.

It is critical to develop an effective and environmental friendly method to prepare TiO_2 NSs with high crystallinity and controllable dimensions. Quasi-titania nanosheets, with well-defined chemical composition of $Ti_{0.91}O_2$, can be synthesized by completely delaminating a lepidocrocite-type layered protonic titanate $H_xTi_{2-x/4}\square_{x/4}O_4 \cdot H_2O$ ($x=0.7$, $\square$: vacancy) into individual layers with tetrabutylammonium (TBA^+) ions using a soft-chemical exfoliation method [20,21]. The 2D colloidal exfoliated $Ti_{0.91}O_2$ NS has a unique structure with an extremely low thickness of 1 nm and a lateral size of micrometers. With such extremely high 2D anisotropy, $Ti_{0.91}O_2$ NS exhibits distinctive physical and chemical properties [22,23]. With these advantages, $Ti_{0.91}O_2$ NSs are expected to be a promising candidate for synthesizing TiO_2 NSs as catalyst used in photocatalytic reactions.

Many approaches have been applied to improve photocatalytic efficiency of TiO_2 by improving its charge separation efficiency, which is the main factor that restricts TiO_2 application. Graphene has recently drawn considerable interest for applications in photovoltaic devices owning to its very light weight, large surface area, and extremely high electron mobility ($\sim$15,000 $cm^2\ V^{-1}\ s^{-1}$) at room temperature [24–26]. It has been demonstrated that incorporation of graphene into TiO_2 NSs greatly facilitates electron transport. However, aggregation and self-assembly of graphene nanosheets in aqueous solution dramatically reduce their specific surface area/active sites owing to their hydrophobicity [27–29]. Graphene oxide (GO), a derivative of graphene, possesses a large number of oxygen functional groups on the nanosheet surface and shares similar advantages with graphene [31–33]. Moreover, light absorption of GO is much smaller than graphene, which favors light irradiation on the surface of TiO_2 [30,31]. As such, GO nanosheets can be an ideal electron acceptor for TiO_2 and can help to enhance e–h separation efficiency. Chen et al. prepared graphene oxide/TiO_2 composites using a modified sol–gel method and evaluated visible light driven photocatalytic performance of graphene oxide/TiO_2 composites for degradation of methyl orange [34]. Sha et al. synthesized GO supported ultrathin TiO_2 NSs using a one-pot hydrothermal method [35]. In this approach, with 5 wt% GO introduced, photocatalytic property was improved due to the increased specific surface area from 4.22 $m^2\ g^{-1}$ to 36.63 $m^2\ g^{-1}$ and accelerated separation of e–h pairs. However, these methods either involve complicated experimental set up or suffer from poor interfacial contact with GO surface due to TiO_2 agglomeration. Therefore, it is necessary to explore a simple and effective approach to solve these issues.

In the present work, ultra-thin TiO_2 NSs are synthesized using a soft-chemical exfoliation method. Photocatalytic activities of the ultra-thin TiO_2 NSs are evaluated via degradation of methylene blue ($C_{16}H_{18}N_3$–SCl, MB) dye under UV light irradiation. Moreover, the effect of GO on photocatalytic property of ultra-thin TiO_2 NSs is explored by simply adding GO aqueous solution to achieve colloidal self-assembly of GO and TiO_2 NSs. The as-prepared GO/TiO_2 NSs demonstrate improved photocatalytic activity due to enhanced charge separation efficiency and large specific surface area. In addition, GO content can be optimized to maximize photocatalytic activity of GO/TiO_2 NSs.

2. Experimental

Lamellar solids of lepidocrocite-type cesium titanate $Cs_xTi_{2-x/4}\square_{x/4}O_4$ ($\square$: vacancy, $x=0.7$) were synthesized using a conventional solid-state calcination method [36,37]. A stoichiometric mixture of Cs_2CO_3 (Alfa Aser, 99.99%) and TiO_2 (anatase, 99%, Sigma-Aldrich) was calcinated with a molar ratio of 1:5.3 at 1073 K for 20 h. After cooling, the products were ground and calcinated repeatedly. Subsequent acid leaching converted them into a protonated form of $H_xTi_{2-x/4}\square_{x/4}O_4 \cdot H_2O$ [20,21]. Protonated titanate was derived through repeated ion exchange of Cs with proton. The resulted powder ($\sim$2 g) was stirred in a 200 ml hydrochloric acid solution with a concentration of 1 mol l^{-1} for 24 h. After Cs extraction was completed via four cycles of ion exchange, the acid-treated product was thoroughly washed with water to remove acid residue and dried under ambient condition.

The as-prepared $H_xTi_{2-x/4}\square_{x/4}O_4 \cdot H_2O$ was treated with tetrabutylammonium hydroxide (TBAOH, $(C_4H_9)_4NOH$, $\sim$40% solution, Fluka) to delaminate into $Ti_{0.91}O_2$ NSs. A weighed amount (2 g) of $H_xTi_{2-x/4}\square_{x/4}O_4 \cdot H_2O$ was shaken vigorously in an aqueous solution (500 ml) of TBA hydroxide at room temperature for two weeks. The amount of TBA hydroxide was 5-fold excess to the exchangeable capacity of $H_xTi_{2-x/4}\square_{x/4}O_4 \cdot H_2O$ (4.12 meq g^{-1}). Typically, 100 ml colloidal suspension of $Ti_{0.91}O_2$ NSs was poured into 100 ml of HCl solution (1 mol l^{-1}). Wool-like precipitates were yielded and the mixture was stirred overnight. After filtration and washing with distilled water, a post-calcination process was necessary for removing organic residues and forming a high-crystalline phase. The obtained solids were then heated at 450 °C in air for 3 h to produce anatase TiO_2 NSs. Single-layer graphene oxide (GO) (ACS Material, LLC) was dispersed in DI water, and then sonicated for 1 h to produce a uniform suspension. The GO/TiO_2 nanosheets are fabricated by mixing various amounts of GO suspension with 5 mg TiO_2 NSs; the weight

percentages of GO were 1 wt%, 3 wt%, 5 wt%, 7 wt%, and 9 wt%.

Crystal structure of TiO_2 NSs was determined by X-ray diffraction (XRD) using a Rigaku MiniFlex diffractometer with Cu Kα radiation operated at 30 kV and 15 mA with a scan rate of 2°/min. Morphology of nanosheets was characterized by a FEI Quanta 3D FEG scanning electron microscope (SEM) at an accelerating voltage of 10 kV. The specific surface area of the protonated titanate and TiO_2 NSs were estimated by nitrogen adsorption/desorption at 77 K on a Quantachrome AS-1 instrument using the 5-point Brunauer–Emmet–Teller (BET) method. High-resolution transmission electron microscopic (HRTEM) images of the as-prepared naosheets were taken using JEOL HRTEM (JEM-1400 electron microscope) with an acceleration voltage of 120 kV. The samples were also observed under a polarized optical microscope using an Olympus BX-51 microscope.

A Spectroline SB-100P UV Lamp (Spectronics Co., USA) emitting a light intensity of 4800 μW cm^{-2} at a wavelength of 365 nm was used to vertically irradiate 50 ml MB aqueous solution in a beaker with an initial concentration of 10 mg l^{-1} and 5 mg TiO_2 nanosheets or GO/TiO_2 nanosheets. The distance between the lamp head and liquid surface was ~10 cm. Before irradiation, the suspensions were added into MB solutions in darkness and the solution was vigorously stirred with a magnetic stirrer for 1 h to establish an adsorption/desorption equilibrium. Subsequently, the solution was irradiated with UV light. Changes in the MB concentration were monitored every 30 min by recording absorption intensity at 664 nm using an UV–vis spectrophotometer (DR/4000U spectrophotometer, HACH). The degradation efficiency is calculated as follows:

$$\eta = (C_0 - C)/C_0 \times 100\% \quad (1)$$

Photocatalytic degradation rate of organic compounds is commonly described by the following Langmuir–Hinshelwood mechanism [38]:

$$\ln(C_0/C) = kt \quad (2)$$

where k is the apparent rate constant of pseudo-first-order, t is the irradiation time, and C_0 and C are the initial and residual concentration of MB solution, respectively.

3. Results and discussion

The colloidal suspension of unilamellar $Ti_{0.91}O_2$ nanosheet is synthesized by delaminating a layered protonic titanate into individual layers with TBA^+ ions intercalated into the interlayer space. Subsequent acid treatment performed on stable colloidal $Ti_{0.91}O_2$ NSs induces reassembly and aggregation of NSs and converts $Ti_{0.91}O_2$ NSs into a gelation form. Thermal annealing is carried out to convert the reassembled gelation to anatase phase. Fig. 1 shows XRD patterns of calcinated cesium titanate, TBA^+-intercalated $Ti_{0.91}O_2$ NS (dried sample), and exfoliated TiO_2 nanosheets after annealing at 450 °C for 3 h. XRD pattern in Fig. 1a shows that the calcinated product is identified as a homogeneous single phase of lepidocrocite-type cesium titanate $Cs_{0.7}Ti_{1.825}\square_{0.175}O_4$ (JCPDS #40-0827) which is synthesized using TiO_2 and Cs_2CO_3 with a molar ratio of 5.3:1 followed by heat treatment at 800 °C for 20 h. As

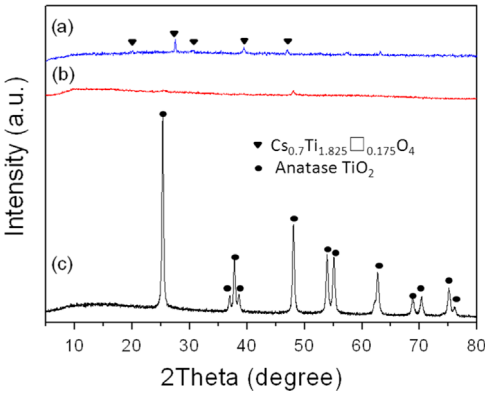

Fig. 1. X-ray diffraction patterns of samples before and after exfoliation: (a) calcinated cesium titanate, (b) TBA^+-intercalated $Ti_{0.91}O_2$ nanosheets (dried sample), and (c) TiO_2 nanosheets obtained via thermal annealing of reassembled $Ti_{0.91}O_2$ nanosheets at 450 °C for 3 h.

reported by Sasaki et al., the protonated titanate $H_xTi_{2-x/4}\square_{x/4}O_4 \cdot H_2O$ is then produced through repeated ion exchange of Cs ions with protons [39]. Afterwards, $H_xTi_{2-x/4}\square_{x/4}O_4 \cdot H_2O$ reacts with TBAOH, intercalating TBA^+ ions into the interlayer space of $H_xTi_{2-x/4}\square_{x/4}O_4 \cdot H_2O$ through ion exchange of TBA with protons. The as-prepared stable colloidal suspension consists of well-dispersed exfoliated nanosheets of hydrated $Ti_{0.91}O_2$. The TBA^+-intercalated $Ti_{0.91}O_2$ NSs are dried at room temperature and display relatively small XRD diffraction peaks as shown in Fig. 1b. This crystalline phase is probably an intermediate phase before forming the final product. Subsequent acid treatment performed on stable colloidal $Ti_{0.91}O_2$ NSs induces reassembly and aggregation of NSs and converts $Ti_{0.91}O_2$ NSs into a gelation form. Thermal annealing is carried out to convert the reassembled gelation to antase phase. Fig. 1c displays XRD pattern of the exfoliated TiO_2 NSs after annealing $Ti_{0.91}O_2$ NSs gelation at 450 °C for 3 h. Typical diffraction peaks at $2\theta = 25.4°$ and $2\theta = 48.0°$ correspond to (101) and (200) in TiO_2 anatase phase (PDF #21-1272, JCPDS). These results indicate that heat treatment converts $Ti_{0.91}O_2$ NSs to crystalline anatase TiO_2 that is subsequently used as photocatalyst for MB degradation.

Morphologies of cesium titanate and TiO_2 NSs are investigated using SEM as shown in Fig. 2. As can be seen from Fig. 2a, cesium titanate sample consists of plate-like particles with widths at sub-micron scale and lengths up to 1 μm. It has been reported that protonated titanate can be stabilized in a suspension containing TBA^+OH^-; in this system, H^+ ions in the interlayer structure of titanate are replaced by much larger TBA^+ ions, increasing the interlayer space of titanate [20,21]. During vigorous stirring, the interlayer space might also be expanded due to intercalation of water and the increased water content in the interlayer space, which significantly reduces electrostatic interaction between neighboring sheets [17]. During the flocculation using HCl solution, TBA^+-intercalated colloidal $Ti_{0.91}O_2$ NS suspension becomes unstable and the nanosheets stack and reassemble together due to the intercalated TBAOH reacting with HCl solution. Fig. 2b shows morphology of TiO_2 NSs obtained via annealing $Ti_{0.91}O_2$ NSs gelation at 450 °C for 3 h. At 450 °C, $Ti_{0.91}O_2$ NSs in the gelation form are restacked together and converted to anatase TiO_2 NSs. These TiO_2 NSs exhibit lateral curling

indicating successful delamination of layered precursor. Importantly, a considerable enhancement of surface area is anticipated by delaminating layered precursor of protonated titanate into single layers with TBA^+ ions. BET surface area analysis shows that surface area of the as-annealed TiO_2 nanosheets is 121.50 $m^2\,g^{-1}$, which is almost 10 times larger than that of protonic titanate (12.98 $m^2\,g^{-1}$), confirming enhanced surface area due to ultra-thin layers of TiO_2 NSs.

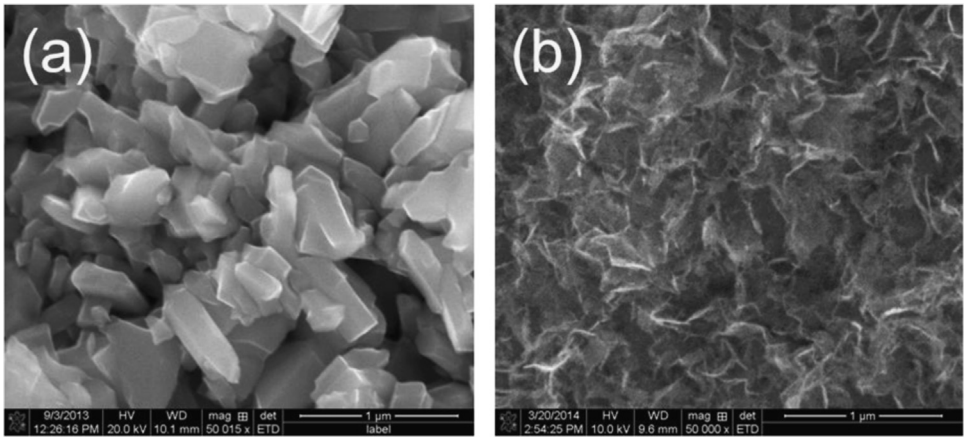

Fig. 2. SEM images of (a) cesium titanate and (b) TiO_2 nanosheets obtained via thermal annealing of reassembled $Ti_{0.91}O_2$ nanosheets at 450 °C for 3 h.

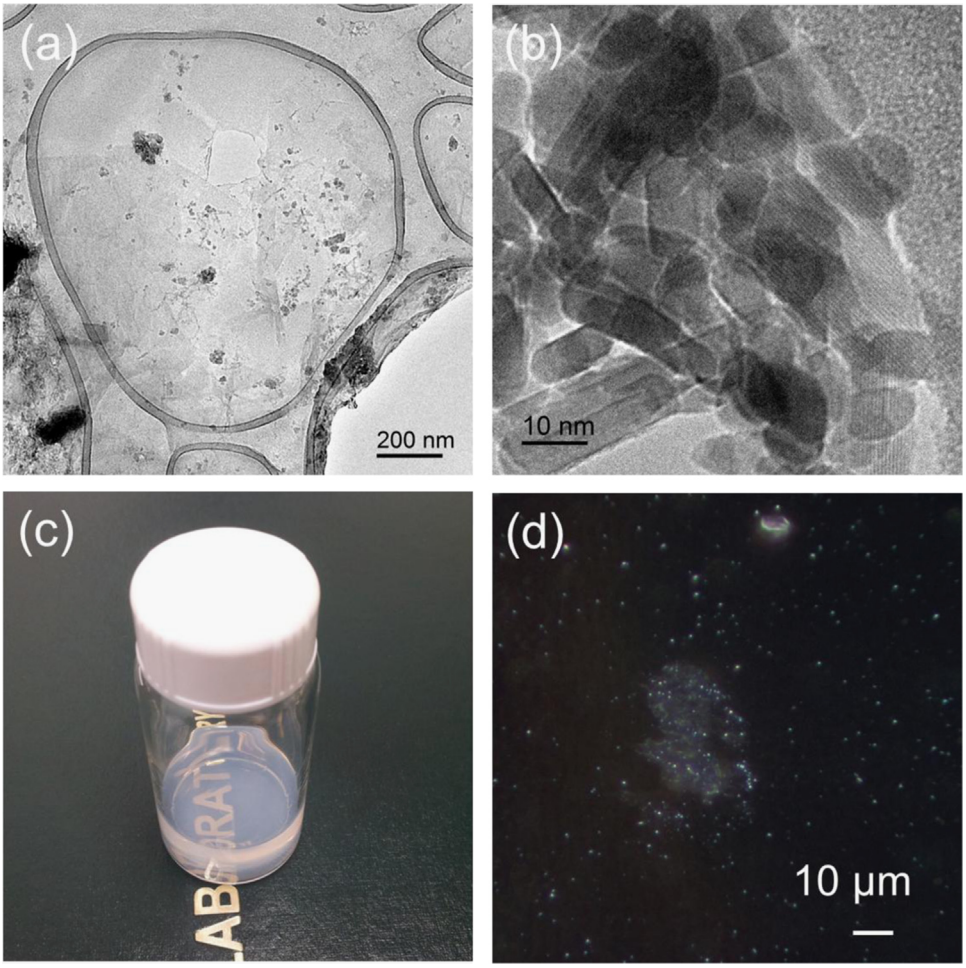

Fig. 3. TEM images of (a) $Ti_{0.91}O_2$ nanosheets, (b) TiO_2 nanosheets, (c) photograph, and (d) polarized microscopy image of TBA^+-intercalated $Ti_{0.91}O_2$ NS colloidal dispersion.

TEM images in Fig. 3a and b further reveal dimensions and structural details of $Ti_{0.91}O_2$ NSs in gelation form and TiO_2 NSs, respectively. Fig. 3a shows TEM image of $Ti_{0.91}O_2$ NSs with a lateral size up to micron scale, which is consistent with the size of the starting material (cesium titanate) that is used to synthesize $Ti_{0.91}O_2$ NSs. Curling and folding of $Ti_{0.91}O_2$ NS into itself indicate its ultra-thin thickness. After heat treatment, a large amount of TiO_2 NSs with a lateral size of 20–100 nm can be clearly observed in Fig. 3b. These TiO_2 NSs are crystalline as lattice fringes are observed in Fig. 3b. It can also been seen in Fig. 3a and b that both $Ti_{0.91}O_2$ NSs and TiO_2 NSs are almost transparent or translucent, indicating their ultra-thin thickness. Moreover, crystallinity of TBA^+-intercalated $Ti_{0.91}O_2$ NS suspension is detected with naked eyes and polarized microscopy due to birefringence of colloids. Fig. 3c shows a photograph of the colloidal suspension containing TBA^+-intercalated $Ti_{0.91}O_2$ NSs, which appears translucent and homogeneous. This colloidal dispersion is stable for several weeks, indicating $Ti_{0.91}O_2$ NSs with ultra-thin thickness are uniformly dispersed and stable in the solvent. Fig. 3d shows a polarized microscopy image of TBA^+-intercalated $Ti_{0.91}O_2$ NS colloidal dispersion, in which crystallinity of TBA^+-intercalated $Ti_{0.91}O_2$ NS suspension is confirmed by birefringence of colloids. However, crystallinity observed by polarized microscopy is not uniform, indicating TBA^+-intercalated $Ti_{0.91}O_2$ NSs may not be completely crystallized. Therefore, a post-calcination process is needed to form a well-crystalline phase.

Photocatalytic activities of different GO/TiO_2 NSs are evaluated by degradation of MB and are compared with that of bare TiO_2 NSs. Under irradiation of UV lamp, blue color of MB solution gradually diminishes, indicating that MB has been degraded by the as-prepared photocatalyst. Fig. 4 compares photocatalytic degradation ratios of MB based on TiO_2 NSs and GO/TiO_2 NSs with various weight ratios of GO (0%, 1%, 3%, 5%, 7%, and 9%). When it is dark (no UV irradiation), it is found that 2.8%, 8.0%, 17.6%, 23.7%, 30.1%, 37.4%, and 40.7% of MB concentration are removed by 1% GO/TiO_2, 3% GO/TiO_2, 5% GO/TiO_2, 7% GO/TiO_2, 9% GO/TiO_2, and TiO_2 NSs, respectively. Owing to strong surface absorption ability of GO, absorption of MB on the photocatalyst increases with the increasing weight ratio of GO. After exposure to UV light for 3 h, degradation of MB in 1% GO/TiO_2, 3% GO/TiO_2, 5% GO/TiO_2, 7% GO/TiO_2, 9% GO/TiO_2, and TiO_2 NSs are 53.2%, 61.3%, 67.0%, 91.2%, 84.1%, and 83.0%, respectively. In particular, the effect of GO on MB degradation efficiency is more distinct for 5% GO/TiO_2, delivering the highest photocatalytic degradation ratio (91.2%) representing 73.1% increase in degradation efficiency compared to bare TiO_2 NS. These results confirm that addition of GO on TiO_2 NSs significantly increases the efficiency of photocatalytic degradation of MB under UV light. Likewise, 9% GO/TiO_2 shows a higher degradation efficiency of 83.0% than that of bare TiO_2 NSs, but slightly lower than that of 5% GO/TiO_2, possibly due to the larger amount of GO added to TiO_2 NSs. The extra amount of GO would lead to graphite-like structure through strong π–π stacking interactions, resulting in slower electron transfer and lower efficiency of MB degradation. Fig. 5 summarizes kinetic behavior of MB photodegradation by TiO_2 NSs and GO/TiO_2 NSs with various weight ratios of GO (1%, 3%, 5%, 7%, and 9%). Corresponding kinetic constants of MB degradation by these nanocomposites are presented in Table 1. The k value of 5% GO/TiO_2 (0.0118 min^{-1}) shows a maximum enhancement of 195% than that of bare TiO_2 NS (0.0040 min^{-1}), indicating that addition of an optmized amount of GO can maximize the photocatalytic efficiency. It can be seen that decomposition of MB becomes significantly faster with the increase of GO weight ratio from

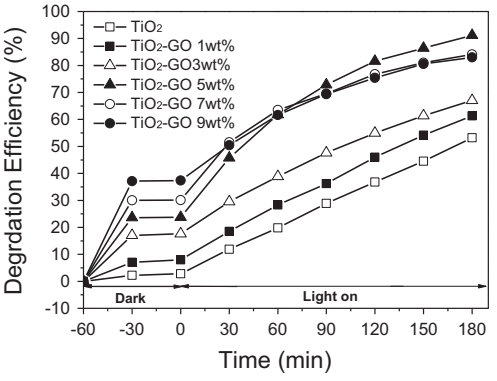

Fig. 4. Photocatalytic degradation ratios of methylene blue degraded by TiO_2 nanosheets and GO/TiO_2 nanosheets with different weight ratios of GO (1%, 3%, 5%, 7%, and 9%).

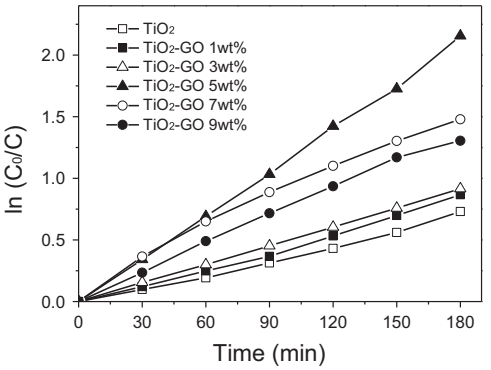

Fig. 5. Photodegradation kinetic curves of methylene blue (MB) degraded by TiO_2 nanosheets and GO/TiO_2 nanosheets with different weight ratios of GO (1%, 3%, 5%, 7%, and 9%), where C_0 and C are the initial and reaction concentrations of MB aqueous solution, respectively.

Table 1
Kinetic characteristics of photocatalytic degradation of methylene blue degraded by TiO_2 nanosheets and GO/TiO_2 nanosheets (1 wt%, 3 wt%, 5 wt%, 7 wt%, and 9 wt%) shown in Figs. 4 and 5.

	$(C_0-C)/C_0$[a] (%)	k[b] (min^{-1})
TiO_2	53.2	0.0040
TiO_2–GO 1 wt%	61.3	0.0048
TiO_2–GO 3 wt%	67.0	0.0051
TiO_2–GO 5 wt%	91.2	0.0118
TiO_2–GO 7 wt%	84.1	0.0081
TiO_2–GO 9 wt%	83.0	0.0074

[a] Photocatalytic degradation ratio of MB degraded by TiO_2 nanosheets and GO/TiO_2 nanosheets.

[b] Apparent rate constant of MB photocatalytic degradation by TiO_2 nanosheets and GO/TiO_2 nanosheets.

1% to 5%, reaching a maximum at 5%, and then becomes slower with the GO weight ratios of 7% and 9%. It is concluded that with an appropriate amount of GO on TiO_2 NSs, efficient charge separation of the photogenerated e–h pairs can be achieved. Compared to photocatalytic activity of other GO/TiO2 NSs synthesized via a hydrothermal method reported in the literature, our GO/TiO_2 NSs exhibit comparable photocatalytic degradation ratio (92.1%) by decomposing the same concentration of MB solution but using much less amount of photocatalyst which is only one-tenth of other's [40]. Moreover, ultra-thin TiO_2 nanosheets synthesized via chemical exfoliation in this work shows much larger surface area (121.50 $m^2 g^{-1}$) than those of TiO_2 nanosheets reported by Sha et al. (4.22 $m^2 g^{-1}$) and Dai et al. (89 $m^2 g^{-1}$) obtained via hydrothermal approaches [35,40]. Last but not least, compared to the commonly used hydrothermal method which involves corrosive hydrofluoric acid, chemical exfoliation in the present work is demonstrated as a safe, environmentally friendly and effective approach.

Photocatalytic reactions take place according to the following mechanism. Electrons of TiO_2 are excited to the conduction band and holes are left in the valence band. Both excited electrons and holes migrate to the surface of TiO_2, where they react with absorbed electron donors and electron acceptors, respectively. In the presence of GO, the excited electrons of TiO_2 transfer from the conduction band to GO [41–43]. Thus, within GO/TiO_2, GO accepts the photoexcited electrons from TiO_2. As such, photocatalytic reactions involved with GO are summarized below:

$$TiO_2 + h\nu \rightarrow e_{cb}^- + h_{vb}^+ \quad (3)$$

$$e_{cb}^- + GO \rightarrow GO\ (e_{cb}^-) \quad (4)$$

$$GO\ (e_{cb}^-) + O_2 \rightarrow \bullet O_2^- \quad (5)$$

$$\bullet O_2^- + H^+ \rightarrow \bullet OOH \rightarrow \bullet OH \quad (6)$$

$$h_{vb}^+ + H_2O \rightarrow \bullet OH + H^+ \quad (7)$$

$$MB + \bullet OH \rightarrow CO_2 + H_2O \quad (8)$$

The enhanced photocatalytic activity of GO/TiO_2 NSs can be attributed to the following factors. First, ultra-thin TiO_2 NSs provide very high surface area and greatly facilitate chemical reactions on their surface by absorbing more organic pollutants. Second, when electrons are excited to the conduction band and holes are left in the valence band, the presence of GO facilitates separation of e–h pairs by trapping more photo-generated electrons from the conduction band of TiO_2 to GO. During this process, e–h recombination is largely suppressed, leading to high photocatalytic activity. Third, the enhanced organic pollutant absorption on GO/TiO_2 NSs contributes to the enhanced photocatalytic activity. The increased surface area with the increased GO content improves absorption of MB and GO. Therefore, the sample with higher GO content of 9% absorbs lager amount of MB in dark due to larger surface area of GO. However, further increase to GO content larger than optimum value would result in a decrease in photocatalytic performance. Although higher GO content absorb more MB, it would limit photocatalytic reaction as the extra GO acting as an e–h recombination center and hinder the diffusion of reactant leading to a lower photocatalytic activity. Also, UV light absorption on TiO_2 would be scarified by the larger absorption of GO. Therefore, photocatalytic efficiency would decrease due to overly large amount of GO.

4. Conclusions

In summary, ultra-thin 2D anatase TiO_2 nanosheets are synthesized using ion exchange between hydrochloric acid and cesium titanate followed by chemical exfoliation via interclalation of TBA^+ ions, HCl treatment, and subsequent heat treatment for applications as photocatalyst for methylene blue degradation. Such TiO_2 NSs resulted from chemical exfoliation of layered pronated titanate and thermal annealing are well-dispersed exhibiting ultra-thin thickness with a lateral size of 20–100 nm. They exhibit high photocatalytic degradation efficiency due to the ultra-thin thickness for electron transfering and large surface area for methylene blue absorption. Moreover, the effect of GO on improving photocatalytic activity of ultra-thin TiO_2 NSs is studied by simply adding GO suspension to achieve colloidal self-assembly. An optimized GO content further improves photocatalytic degradation efficiency due to enhanced electron–hole seperation and increased surface area provided by GO. The present work confirms a simple but effective approach by combing graphene oxide with TiO_2 nanosheets synthesized via exfoliation for application as highly-efficient photocatalyst for methylene blue degradation.

Acknowledgment

This work is supported by LABOR – RCS grant LEQSF (2011-14)-RD-A-13. The authors want to thank for Materials Characterization Center at LSU for using XRD and SEM. X. N. Luan also acknowledges LSU Graduate School Enrichment Award.

References

[1] M. Gratzel, Coord. Chem. Rev. 111 (1991) 167–174.
[2] A. Kay, M. Gratzel, J. Phys. Chem. 97 (1993) 6272–6277.
[3] O.K. Varghese, M. Paulose, C.A. Grimes, Nat. Nanotechnol. 4 (2009) 592–597.
[4] M.D. Ye, X.K. Xin, C.J. Lin, Z.Q. Lin, Nano Lett. 11 (2011) 3214–3220.
[5] X. Luan, D. Guan, Y. Wang, J. Phys. Chem. C 116 (2012) 14257–14263.
[6] O.K. Varghese, D.W. Gong, M. Paulose, K.G. Ong, C.A. Grimes, Sens. Actuators B: Chem. 93 (2003) 338–344.
[7] E. Sennik, Z. Colak, N. Kilinc, Z.Z. Ozturk, Int. J. Hydrog. Energy 35 (2010) 4420–4427.
[8] H.F. Lu, F. Li, G. Liu, Z.-G. Chen, D.-W. Wang, H.-T. Fang, G.Q. Lu, Z.H. Jiang, H.-M. Cheng, Nanotechnology 19 (2008) 1–7.
[9] Z. Zhang, P. Wang, Energy Environ. Sci. 5 (2012) 6506–6512.
[10] K. Shankar, G.K. Mor, H.E. Prakasam, S. Yoriya, M. Paulose, O.K. Varghese, C.A. Grimes, Nanotechnology 18 (2007) 065707.
[11] S. Rani, S.C. Roy, M. Paulose, O.K. Varghese, G.K. Mor, S. Kim, S. Yoriya, T.J. LaTempa, C.A. Grimes, Phys. Chem. Chem. Phys. 12 (2010) 2780–2800.
[12] D. Losic, S. Simovic, Expert Opin. Drug Deliv. 6 (2009) 1363–1380.

[13] D. Guan, C. Cai, Y. Wang, J. Nanosci. Nanotechnol. 11 (2011) 3641–3650.
[14] J. Tschirch, D. Bahnemann, M. Wark, J. Rathousky, J. Photochem. Photobiol. A: Chem. 194 (2008) 181–188.
[15] M. Wark, J. Tschirch, O. Bartels, D. Bahnemann, J. Rathousky, Microporous Mesoporous Mater. 84 (2005) 247–253.
[16] Y. Sakatani, D. Grosso, L. Nicole, C. Boissiere, G. Soler-Illia, C. Sanchez, J. Mater. Chem. 16 (2006) 77–82.
[17] R.Z. Ma, Y. Bando, T. Sasaki, J. Phys. Chem. B 108 (2004) 2115–2119.
[18] J. Yu, J. Fan, K. Lv, Nanoscale 2 (2010) 2144–2149.
[19] L. Zhao, J. Li, Y. Shi, S.M. Wang, J.H. Hu, B.H. Dong, H.B. Lu, P. Wang, J. Alloys Compd. 575 (2013) 168–173.
[20] T. Sasaki, M. Watanabe, J. Am. Chem. Soc. 120 (1998) 4682–4689.
[21] T. Maluangnont, K. Matsuba, F. Geng, R. Ma, Y. Yamauchi, T. Sasaki, Chem. Mater. 25 (2013) 3137–3146.
[22] T. Sasaki, M. Watanabe, J. Phys. Chem. B 101 (1997) 10159–10161.
[23] N. Sakai, Y. Ebina, K. Takada, T. Sasaki, J. Am. Chem. Soc. 126 (2004) 5851–5858.
[24] K.S. Novoselov, A.K. Geim, S.V. Morozov, D. Jiang, Y. Zhang, S.V. Dubonos, I.V. Grigorieva, A.A. Firsov, Science 306 (2004) 666–669.
[25] A.K. Geim, K.S. Novoselov, Nat. Mater. 6 (2007) 183–191.
[26] K.S. Novoselov, A.K. Geim, S.V. Morozov, D. Jiang, M.I. Katsnelson, I.V. Grigorieva, S.V. Dubonos, A.A. Firsov, Nature 438 (2005) 197–200.
[27] Y. Xu, K. Sheng, C. Li, G. Shi, ACS Nano 4 (2010) 4324–4330.
[28] D. Li, M.B. Mueller, S. Gilje, R.B. Kaner, G.G. Wallace, Nat. Nanotechnol. 3 (2008) 101–105.
[29] S. Stankovich, D.A. Dikin, R.D. Piner, K.A. Kohlhaas, A. Kleinhammes, Y. Jia, Y. Wu, S.T. Nguyen, R.S. Ruoff, Carbon 45 (2007) 1558–1565.
[30] D.R. Dreyer, S. Park, C.W. Bielawski, R.S. Ruoff, Chem. Soc. Rev. 39 (2010) 228–240.
[31] J. Kim, F. Kim, J. Huang, Mater. Today 13 (2010) 28–38.
[32] Y. Matsumoto, M. Koinuma, S. Ida, S. Hayami, T. Taniguchi, K. Hatakeyama, H. Tateishi, Y. Watanabe, S. Amano, J. Phys. Chem. C 115 (2011) 19280–19286.
[33] X. Yang, Y. Tu, L. Li, S. Shang, X.-M. Tao, ACS Appl. Mater. Interfaces 2 (2010) 1707–1713.
[34] C. Chen, W. Cai, M. Long, B. Zhou, Y. Wu, D. Wu, Y. Feng, ACS Nano 4 (2010) 6425–6432.
[35] J. Sha, N. Zhao, E. Liu, C. Shi, C. He, J. Li, Carbon 68 (2014) 352–359.
[36] I.E. Grey, I.C. Madsen, J.A. Watts, L.A. Bursill, J. Kwiatkowska, J. Solid State Chem. 58 (1985) 350–356.
[37] I.E. Grey, C. Li, I.C. Madsen, J.A. Watts, J. Solid State Chem. 66 (1987) 7–19.
[38] R.W. Matthews, J. Phys. Chem. 91 (1987) 3328–3333.
[39] T. Sasaki, M. Watanabe, H. Hashizume, H. Yamada, H. Nakazawa, J. Am. Chem. Soc. 118 (1996) 8329–8335.
[40] K. Dai, L. Lu, Q. Liu, G. Zhu, Q. Liu, Z. Liu, Dalton Trans. 43 (2014) 2202–2210.
[41] B. Jiang, C. Tian, W. Zhou, J. Wang, Y. Xie, Q. Pan, Z. Ren, Y. Dong, D. Fu, J. Han, H. Fu, Chemistry 17 (2011) 8379–8387.
[42] G. Williams, B. Seger, P.V. Kamat, ACS Nano 2 (2008) 1487–1491.
[43] H. Zhang, X. Lv, Y. Li, Y. Wang, J. Li, ACS Nano 4 (2010) 380–386.